Journal of the European Ceramic Society **19** (1999) 1731–1739

PII: S0955-2219(98)00276-3
0955-2219/99/$ - see front matter

Influence of Electromagnetic Fields on the Microstructure of Precipitated Calcium Phosphate Nanometric-Grains

Dario T. Beruto* and Marino Giordani

Institute of Materials Science and Engineering, Faculty of Engineering, University of Genoa, Piazzale J. F. Kennedy, Fiera del Mare Pad. D, I 16129 Genova GE, Italy

(Received 12 August 98; accepted 13 November 98)

Abstract

Extremely low frequency electromagnetic fields (EM-ELF) of 3 mT and 1300 Hz in frequency were applied during spontaneous precipitation processes of calcium phosphates mixtures from their supersaturated aqueous solutions of calcium chloride and sodium phosphates. At the temperature of 37° C and at an aqueous solution with pH 7·4, for any total precipitation time ranging between 15 min and 5 h, the precipitated solid phase is formed by octacalcium phosphate (OCP) and by non-stoichiometric hydroxyapatite (ns-OHAp). The EM-ELF forces do not produce any effect in changing the chemical composition of the precipitated mixture. For any precipitation time the powders obtained under the action of the EM-ELF fields are characterised by a specific surface area values which are lower then the ones corresponding to samples obtained without EM-ELF applied by a percentage ranging between 18 and 36%. The crystallites sizes of both samples range between 10 and 20 nm, but the EM-ELF samples are characterised by an average crystallites size which is about the 40% bigger than that of one concerning the specimen precipitated without any EM-ELF applied. Experimental evidences are given to support the hypothesis that the action of the EM-ELF fields is active at the beginning of the precipitation process when the calcium phosphate particles are still in a colloidal-like status. Critical discussions, based on a theory that the authors previously described, establish that the dimension of the particles on which the applied exogenous field can have an effect is of the order of 0·1 nm. © *1999 Elsevier Science Limited. All rights reserved*

*To whom correspondence should be addressed. Fax: + 39-010-353-6034; e-mail: iism@unige.it

Keywords: electromagnetic fields, precipitation, powders, chemical preparation, surfaces, apatite.

1 Introduction

In our previous publication,[1] dealing with the effect of the low frequency electromagnetic field (EM-ELF) on crystal growth from solutions, we made a survey of experimental and theoretical data that allow to explain the action of weak electromagnetic forces on the microstructure of precipitates powders like barium oxalate[2] and calcium carbonate.[3] In those precipitation processes the nucleation step was followed by a crystal growth stage that ultimately yields to a precipitated phase with a unique crystalline habit and/or to a mixture of powders with different crystalline phases, but with equal chemical nature. It is interesting to explore whether or not there is any effect of the applied exogenous EM-ELF field on the microstructure of the precipitating mixture formed by powders with different crystalline phases and with different chemical nature. This is a rather attractive class of reactions, which include the production of powders used as raw materials for humidity ceramic sensors,[4] as well as for bioceramics.[5]

In this paper we will investigate primarily if extremely low frequency electromagnetic field of 3 mT and 1300 Hz will have any effect on the microstructure features of precipitated powders formed by a mixture of octacalcium phosphates (OCP) and nonstoichiometric hydroxyapatite (ns-OHAp) obtained from a spontaneous precipitation process.[6–8]

Preliminary results on this precipitation process have been already obtained.[1,9] In this paper we complete the previous studies in order to achieve a better knowledge of this complex process. In

particular, the spontaneous precipitation process used as the reference[6–8] will be explored to clarify the chemical composition of the precipitated powders and their microstructure at the nanometric level.

Furthermore, on the grounds of the model proposed to explain the effects of the EM-ELF fields[1] on the crystal growth, the relationship between the size of the dispersed particles and the probability that on such particles the electromagnetic forces being active will be investigated.

The precipitated system is one of biological interest[9,10] and thus the results of the effect of the EM-ELF fields on such a system can yield information potentially useful for the biomineralization processes.[11–18]

2 Materials and Experimentals Procedure

2.1 EM-ELF apparatus

The experimental apparatus used for the precipitation processes reported in this work is a modified version of that already described in our previous publications.[2] Basically this instrument (see Fig. 1) is designed to carry on simultaneously precipitation processes in two symmetrical beakers respectively exposed (active, $B \neq 0$) and not exposed (passive, $B = 0$) to the EM-ELF field. Since the solution is static (i.e. its barycentric rate is equal to zero) as a source for the electromagnetic field an alternating current flowing in Helmoltz coils was chosen. A first source of experimental errors, which can be introduced by these instruments, is the extra-thermal effect in the systems, due to the electric current flowing into coils. To avoid this inconvenience the same liquid solutions have been poured into two vessels placed midway into two coils. On the active coils side (Helmoltz), the alternating current generated by a power amplifier (driven by a sinusoidal signal generator with a frequency of 1300 Hz) flows, to produce a preselected constant a.c. magnetic field B superimposed to the earth's field (in our case 3 mT). On the passive coils side (Dummy) wires of the same diameter and loop as utilised for the active side have been used, but the loop winding has been such as to generate an internal B field equal to zero. Accordingly, if any extrathermal effect due to the flow of the electric current is produced, this is equal for both experiments carrying on with and without ELF applied field.

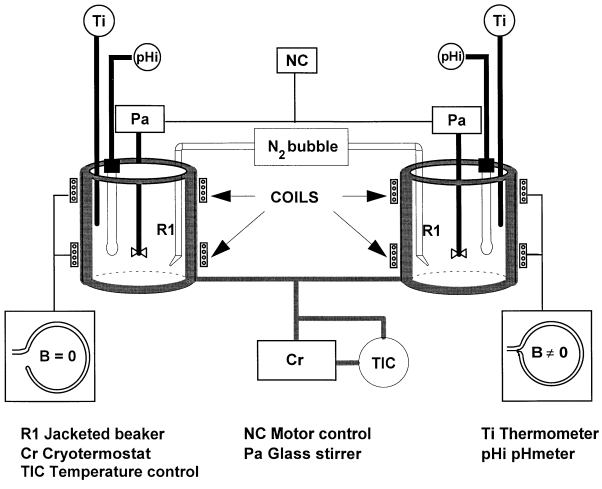

Fig. 1. Experimental apparatus with Helmoltz/Dummy-coils source.

2.2 Precipitation method

Reagent grade materials were used throughout the experiments. The precipitation tests were performed with and without EM-ELF fields applied accordingly to the following procedure. Supersaturated solution obtained mixing 225 ml of calcium chloride (0·04 M), 225 ml of Na_2HPO_4 (0·036 M) and 300 ml of distilled water at 37°C and at a pH equal to 7·4[6–8] were placed in a water-thermostat double walled vessel. At the beginning of the precipitation process the solution pH showed a tendency to decrease, thus to keep it at a constant value the required amount of tris-idroxymethyl-aminomethane, which exerts a buffering effect, was introduced.[19] Calomel-glass electrode was used to measure the solution pH, before and after each experiment the electrode systems were standardised. In the course of the precipitation process the observed experimental fluctuations of the pH value do not exceed the sensitivity of the instrument equal to $\pm 0{\cdot}01$. The solutions were stirred with a glass stirrer at about 300 rpm, and CO_2 free nitrogen gas was bubbled through the vessels to exclude carbon dioxide. The total precipitation time was set different for each precipitation process. The values selected were 15, 60, 120 and 300 min. Control of the liquid phase with the precipitating agent showed that the precipitation reactions were complete within 5 min. The obtained precipitates were first filtered through Millipore cellulose filters of 0·45 μm pore size and washed with cold water until free from chloride within an operation time of about 30 min. Then they were dried in vacuum at room temperature for a total time of about 3 days and kept in a dessicator for further analysis. To estimate experimentally all possible source of errors that can occur in these precipitation processes and in the subsequent washing and drying procedures, each experiment was repeated twice and the surface area values of the products obtained under *the same* experimental conditions were evaluated (see below). The maximum difference in these measurements was assumed as the error intrinsically related to the incertitude of the adopted experimental methods.

2.3 Precipitate phases analysis

To investigate the microstructure of the precipitate phases from the level of the nanometric scale to that of the micrometric one, SEM observations and N_2-adsorption–desorption isotherms at $-195°C$[20] were made for all the prepared samples. For SEM observations, in the range of magnification between 10^3 and 200×10^3, 20 nm of gold[21] was evaporated on the powder samples and then placed into the high vacuum SEM chamber using an accelerating voltage of 20 KV.

N_2-adsorption–desorption isotherms were carried-out in a symmetrical thermogravimetric apparatus with sensitivity equal to 10^{-6} g and in controlled gaseous environment conditions. Experimental details of this apparatus have been described elsewhere.[20] From these measurements, applications of BET theory[22] allow to obtain sample specific area value, while analysis on the entire adsorption and desorption cycle[23] yields values of the sample porosity and of the pore size distribution within the pores range equal to about 1–50 nm. Agglomeration of powders, eventually due to their manipulation from the filtration step to the N_2-adsorption one, do not influence the measurements of specific surface as well as the sample porosity and the pore size distribution for the following reasons. First the N_2 molecules have an average radius of about 0·4 nm,[23] while the possible agglomeration phenomena are effective at the micrometric scale, thus the nitrogen molecules are insensitive to what happens on the sample macroscale.[24] Secondly the investigated samples are characterised by surface area value of the order of 100 $m^2\,g^{-1}$; any variation in particle agglomerate size, ranging in the microns level, is included in the usual experimental error assumed to be equal to $\pm5\%$ of the surface area measured.[22] To investigate the chemical nature of the produced solid products, thermal analysis (TG) and differential scanning calorimetric (DSC)[25] were coupled with XRD measurements and energy disperse spectroscopy technique (EDS). For the EDS experiments the powders were pressed into small cylindrical pellets in a stainless-steel die at an applied pressure of about 350 MPa for 3 min. Each pellet was about 6 mm in diameter and 2 mm in length. The pellets were coated in vacuum with about 5 nm of carbon. Accelerating voltage was set at 15 keV and spot size at 4 μm. The collected spectra were compared with those obtained from certified natural apatite. Composition was based on an average calculated from at least five analyses carried out on a surface of about 30 mm^2. For the TG and the DSC measurements about 20 mg of sample were placed in a platinum crucible inside a thermobalance that allows to obtain simultaneously the TG and the DSC traces. The samples were heated at a rate of 10°C min^{-1} in dry air atmosphere up to the temperature of 950°C. Kaolin powders (100 mesh) were used as a reference system.[25] When phase transformations were recorded by the DSC traces, for a number of experiments, cycling between the observed peak of temperature (450–700°C) were made to test the reversibility and/or irreversibility of the transformation. Before and after each observed thermal effects, powders X-ray diffraction (XRD) analysis were carried out to evaluate the crystalline phases composition. For all XRD measurements, both on the heated and the precipitated samples, the extra-ray source was provided by CoK_α radiation using a Fe filter, with an applied voltage of 40 kV, an intensity current of 20 mA, a CPS range of 4×10^2, a scan speed of 1° 2θ min^{-1} and a scan range between 10 and 60°.

3 Results and Discussion

3.1 Spontaneous precipitation processes

Figure 2 illustrates XRD diffraction patterns concerning the precipitated powders obtained for a total precipitation time respectively equal to 15 min (line a), 60 min (line b) and 120 min (line c). The JCPDS stick patterns[26] concerning the OHAp and OCP crystalline phases have been reported for sake of comparison with our products. It is possible to observe that increasing the total precipitation period of time does not change the position of the diffraction peaks, but it increases the area of the peaks defined by 2θ value ranging between 36 and 40°. The obtained XRD diffraction patterns are different from the ones corresponding to high purity OHAp and OCP phases (see bottom and top of Fig. 2), as well as they are too different from the XRD traces of other single calcium phosphates phases reported in JCPDS tables.[26] This spectra might be ascribed to poor crystalline OHAp, but, as the EDS analysis is showing, the average Ca/P ratio for the obtained precipitate powders is equal

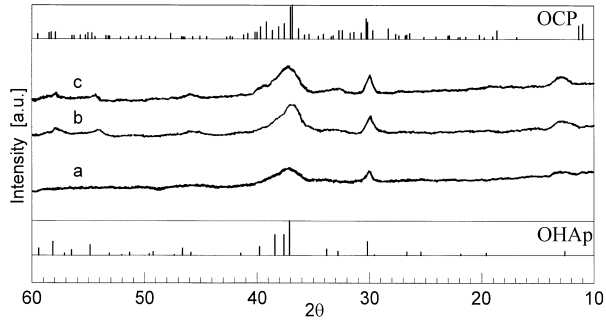

Fig. 2. XRD diffraction patterns of precipitated powders obtained for different total precipitation time (line a = 15 min, line b = 60 min, line c = 120 min).

to $1{\cdot}49 \pm 0{\cdot}01$, very far indeed from the value expected for any kind of hydroxyapatite.[16] Very reasonably these powders are formed by a mixture of calcium phosphates.

To establish the chemical composition of the precipitated mixtures a number of techniques can be used,[27] in the following, we illustrate the results obtained by a combination of thermal analysis, XRD and EDS techniques.

Figure 3 gives the thermogravimetric analysis (TG) and the simultaneous differential scanning calorimetric (DSC) for a typical precipitated sample in the temperature range between 100 and 950°C with a heating rate equal to 10°C min^{-1} and in dry air atmosphere. The samples were dried before the heating treatment, so that no weight loss was recorded before 100°C. Even if the detailed interpretation of the thermal decomposition phenomena illustrated in Fig. 3 is a rather complex matter,[16] for our purpose the following considerations are easily to be derived. At 650°C, after the irreversible exothermic transformation (point A in Fig. 3), the XRD analysis on the heated solid-products (see Fig. 4, line a) showed the presence of the phases ns-OHAp and β-TCP At the end of the thermal decomposition, 850°C, the observed XRD solid composition is only made by β-TCP (Fig. 4, line b).

The total weight loss, taking into account all source of experimental errors, is equal to $6{\cdot}7 \pm 0{\cdot}1\%$. Partitioning of this weight loss between the two reactions:

$$2Ca_8H_2(PO_4)_6 5H_2O = Ca_3(PO_4)_2 + Ca_2P_2O_7 + 6H_2O \qquad \Delta W = -10{\cdot}99\% \tag{1}$$

and:

$$Ca_5(PO_4)_3OH = Ca_3(PO_4)_2 + CaO + H_2O \qquad \Delta W = -1{\cdot}79\% \tag{2}$$

yields to the result that the composition of the initial mixture is made by 44% of ns-OHAp and by 56% of OCP. If so the predicted Ca/P ratio would be equal to 1·48. The EDS experimental data show that the Ca/P ratio is equal to $1{\cdot}49 \pm 0{\cdot}01$ in quite good agreement with the one predicted by eqns (1) and (2).

Thus on the basis of the above reported results we can conclude that the precipitated mixtures obtained from the spontaneous precipitation process here illustrated, are formed by OCP and ns–OHAp. These results are in agreement with previous studies already published and concerning the case where the solution is unstable with respect to all the phases in the near neutral or alkaline part of the $Ca(OH)_2$–H_3PO_4–H_2O phase diagram.[16]

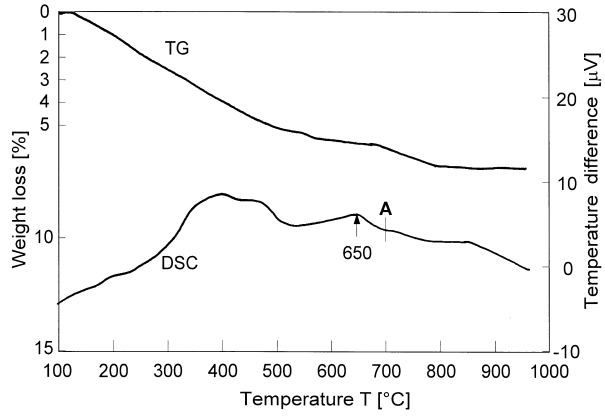

Fig. 3. DSC and TGA curves of precipitated powders. Heating rate = 10 K min^{-1} in dry air atmosphere. Point A (973 K) represents the adopted temperature for heat treatment.

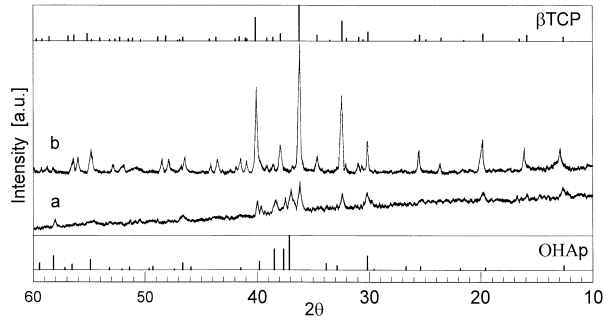

Fig. 4. XRD diffraction patterns of precipitated powders after annealing at 973 K (line a) and at 1123 K (line b) in dry air atmosphere.

3.2 Effect of the EM–ELF fields

A first question to be addressed is that concerning the effect of the applied EM-ELF field on the chemical nature of the precipitated powders. For the sake of simplicity let us name with EM-OCP/OHAp, the samples that have been exposed to the electromagnetic field and with OCP/OHAp the mixtures not exposed but obtained under the same experimental precipitation conditions. EDS measurements show that the average Ca/P ratio value is equal to $1{\cdot}48 \pm 0{\cdot}01$ for the EM-OCP/OHAp mixtures and to $1{\cdot}49 \pm 0{\cdot}01$ for the OCP/OHAp ones. The difference between the two average values is not significant because the maximum experimental scattering established within each set of measurements has been turned-out equal to 0·02. In the temperature range 100–950°C, thermogravimetric experiments on this set of precipitate powders yield a total weight loss equal to the $6{\cdot}5 \pm 0{\cdot}1$ and to $6{\cdot}7 \pm 0{\cdot}1\%$ in weight, respectively, for the EM mixtures and for the other ones. From the above reported EDS-Ca/P data, the

amount of OCP product appears to be equal to 51% in the EM-OCP/OHAp powders, and 55% in the OCP/OHAp one. The difference between these percentage values has no experimental meaning. Indeed if one assumes that the usual thermobalance error is of the order of 2%, the error in the Ca/P ratio appears to be greater than 4%. Summing up all these observations it seems reasonable to conclude that the applied weak electromagnetic fields *do not have* any effect on the bulk-chemical composition of the precipitated mixtures.

Let us concentrate now on the possible influence that the applied field might have on the microstructure of the precipitate powders. Considering first the microstructure scale included in the range 10^{-1}–10 μm. Such observations are easily done by low magnification SEM (×l0000) measurements on the precipitated dried powders. The results concerning both the OCP/OHAp and the EM-OCP/OHAp samples show that the precipitate powders are formed by porous grains-aggregates of irregular shape and average dimension of about 3 μm. Thus at least at the micron structure level the effect of the weak electromagnetic force does not produce any significant change.

Figures 5 and 6 are typical results obtained through higher magnification SEM (×200 000) observations on both sets of samples treated with different ultrasonic dispersion polar techniques in not polar liquid,[21] before the microscopic analysis. As it is possible to observe, the grains are still aggregate, and the average dimension of the single grains can clearly be set in the range between 10 and 20 nm. TEM observations still at ×200 000 magnification yield to the same results.

To derive a difference between the microstructure of the OCP/OHAp samples and the microstructure of the EM-OCP/OHAp ones from these higher magnification observations is a tough task. Thus to decide if the EM-ELF fields have any effect on the microstructure features of the treated precipitated samples, other techniques[9,28] need to be explored.

Figure 7 shows the N_2-adsorption–desorption isotherm loop at −195°C for two typical EM-OCP/OHAp (loop A) and OCP/OHAp (loop B) samples obtained after a total precipitation period of 2 h. Accordingly to Brunuaer's classification[23] the adsorption isotherms above reported are IV-type isotherms. This implies that the samples are porous and that the capillary cavities have an average size dimension included in the range between 2 nm and 30 nm (mesoporosity range).[23]

Figure 8 (curves a and b) illustrates the evolution of the specific surface area derived from adsorption isotherms like the ones reported in Fig. 7 and corresponding to different EM-OCP/OHAp and

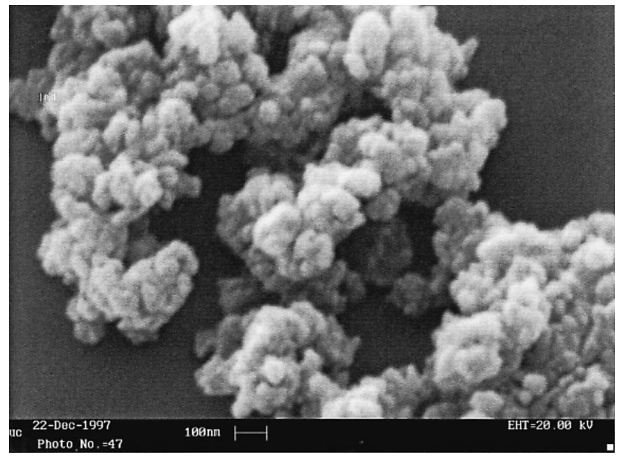

Fig. 5. SEM micrograph of EM-OCP/OHAp powder.

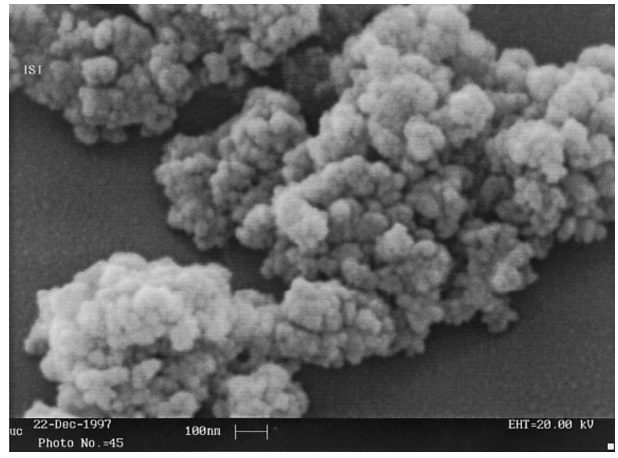

Fig. 6. SEM micrograph of OCP/OHAp powder.

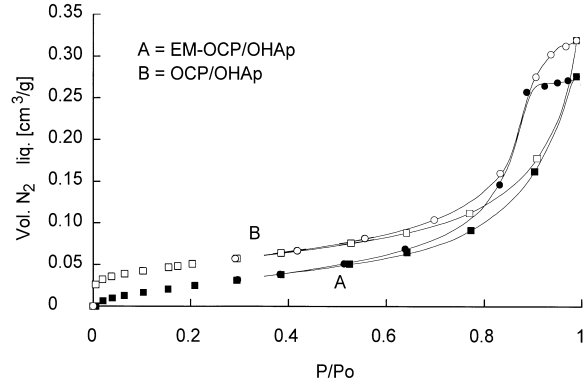

Fig. 7. N_2-adsorption–desorption isotherms loop at 78 K for two typical EM–OCP/OHAp (loop A) and OCP/OHAp (loop B) samples obtained after a total precipitation time equal to 2 h.

OCP/OHAP samples obtained at different precipitation time. As it is possible to observe for both sets of samples the correspondent specific surface area values are decreasing as the total precipitation time is increasing, but the values concerning the EM-OCP/OHAp samples (curve a) are always lower than the correspondent OCP/OHAp ones

(curve b). The decreasing behaviour of both curves is very reasonable due to the precipitated grain size growth process that is occurring as the precipitation time is increasing.[29] However it is interesting to observe that, for any pre-selected precipitation time, the values of the EM-OCP/OHAp samples surface are always lower then those of the OCP/OHAp mixtures by an amount that is ranging between 18 and 36%. The maximum global experimental error that has been found in these measurements, comparing the surface area values of samples precipitated, washed and dried under *the same* experimental conditions, do not exceed 10%. Thus an observed difference of 18–36% in the S_{BET} values is a reliable evidence that the EM-ELF forces do produce some effect on the microstructure of the samples precipitated when the EM-ELF fields are applied.

These experimental evidences are further supported by the results of the pore size distributions derived from the N_2 desorption isotherms[30] accordingly to the Orr and Dalla Valle method.[31]

Figure 9 shows the pore size distribution for the EM-OCP/OHAp samples (curve A) and for the OCP/OHAp ones (curve B) corresponding to the data illustrated in Fig. 7. As it is possible to observe, the samples that have been precipitated under the action of EM-ELF forces are characterised by pores with an average dimension (6 nm) which is slightly greater than that concerning obtained without any EM-ELF field applied (5 nm). This tendency has been confirmed by the comparison of the pore size distribution of all other samples precipitated at the same time with or without the EM-ELF field applied.

For agglomerate powders like those illustrated here between the average dimension of the pores and the crystallites average dimensions, the Tomeikeieff relationship can be applied.[32] Thus it is possible to write:

$$r_p = \beta r_c P/(1 - P) \qquad (3)$$

r_p, r_c being, respectively, the average radius of the pores and of the crystallites, P the experimental agglomerates porosity, and β a constant value which is dependent upon the crystallites geometry here assumed equal to 1. Application of eqn (3) to the data of Figs 7 and 9 allows to evaluate an average crystallites dimension equal to 14 nm for the EM-OCP/OHAp samples and to 10 nm for the OCP/OHAp mixtures. SEM and TEM observations at ×200 000 magnification confirmed that these results are in the range of the crystallites dimension directly observed (10–20 nm), but the pore size analysis allows to observe that the average dimension of the crystallites concerning the EM-ELF samples

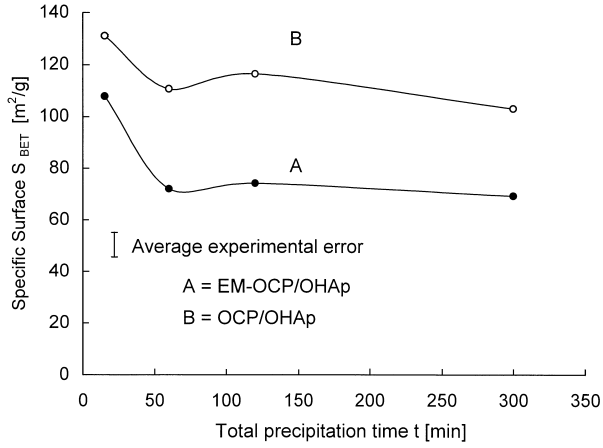

Fig. 8. Evolution of the specific surface area S_{BET} Versus the total precipitation time for EM-OCP/OHAp mixtures (curve A) and for OCP/OHAp ones (curve B).

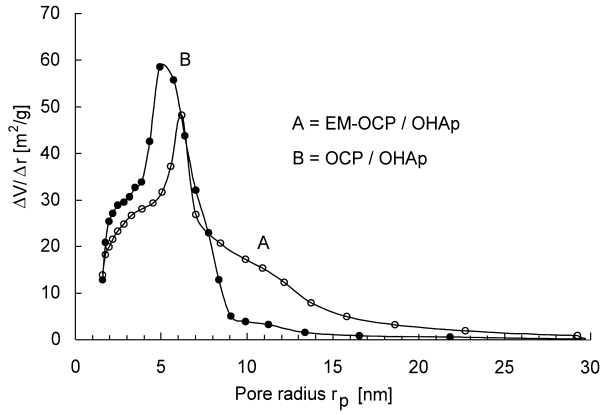

Fig. 9. Pore size distribution for two typical EM-OCP/OHAp (line A) and OCP/OHAp (line B) samples obtained after a total precipitation time equal to 15 min.

is slightly greater then that concerning the OCP/OHAp mixtures. As matter of comparison it can be easily shown that a difference of 4 nm in the average crystallites size dimension is sufficient to explain the experimental observation that the specific surface values of the EM-ELF samples are lower than the ones concerning the mixtures obtained without any EM-ELF field applied, by an amount ranging between 18 and 36%.

An interesting question to be asked is that concerning the time scale and the microstructure scale on which the EM-ELF forces are interacting with the calcium phosphates particles. In seeking data for studying this point let us consider the difference ΔS, between the S_{BET} values plotted in Fig. 8 for any precipitation time. Figure 10 illustrates the result. Within the experimental error, ΔS is constant for a total precipitation time included between 15 and 300 min. This evidence strongly suggests that the EM-ELF forces are active during a period of total precipitation time shorter than 15 min (shadow zone in Fig. 10). The analysis of the liquid phase in which the precipitation process is occurring tells us that the solid phase formation

is completed within 5 min (see Experimental section), thus the effect of the EM-ELF electromagnetic forces should be exerted on particles with a dimension that is much smaller than the one corresponding to the precipitate powders after 15 min. During this period of time most of the formed product can be in a colloidal like status. Thus the effect of the EM-ELF electromagnetic forces should be due to the interactions between electromagnetic forces and colloidal-like particles in the early beginning of their formation processes. This means going back to the regions where the nucleation processes of the precipitate crystallites are important. To obtain experimental evidence in these regions is a tough item basically for two reasons. The first one is that the rate of nucleation period is quite often a very fast reaction,[33] the second one is that it is experimentally difficult to make observations on the dimension of objects in solutions that might be of the order of 10^{-1} nm.

As a matter of discussion let us recall briefly a physical model that we have already proposed[1] as a possible one to explain the effect of the EM-ELF fields on the kinetics and on the microstructure evolution of nuclei and/or the colloidal particles dispersed in the aqueous solution. Figures 11(a) and (b) illustrates the model before [section (a) in Fig. 11] and after [section (b) in Fig. 11] the exposure of the aqueous solution/dispersion to the EM-ELF fields. Around each particle it is assumed that a uniform charged density exists. Due to the action of the external electric field Φ the charged density is modified by a polarisation effect [Fig. 11(b)], that it will strain the total interfacial solid/liquid layer around each particle. If the applied field has a low frequency it is assumed that the new configuration be stable over a certain period of time, during which agglomeration and/or other reactive processes can occur. Let us define σ_u the total interfacial energy "per" particle for the unstrained configuration [Fig. 11(a)]. The probability of polarisation, θ_p, will be:

$$\theta_p = \sigma_s/(\sigma_s + \sigma_u) \tag{4}$$

where σ_s, is the total interfacial energy-increasing due to the effect of the EM-ELF fields.

For an applied electromagnetic field of 3 mT at frequency ν of 1300 Hz, the value of σ_s, has been evaluated equal to about 100 meV.[34] This value has been recently confirmed by calculations on a simple theoretical model[1] and it depends only on the transfer of the electrical charge at the solid/liquid interface. The unstrained interfacial energy value can be written as:

$$\sigma_u = \sigma_{s1} 4\pi r^2 \tag{5}$$

being σ_{s1} the experimental solid/liquid interfacial energy per m^2 in meV and r the nuclei radius in m. Substitution of eqn (5) into eqn (4) shows that the probability θ_p is decreasing as the radius of particle is increasing, thus the effect of EM-ELF fields tends to be negligible as the particles dimension increases.

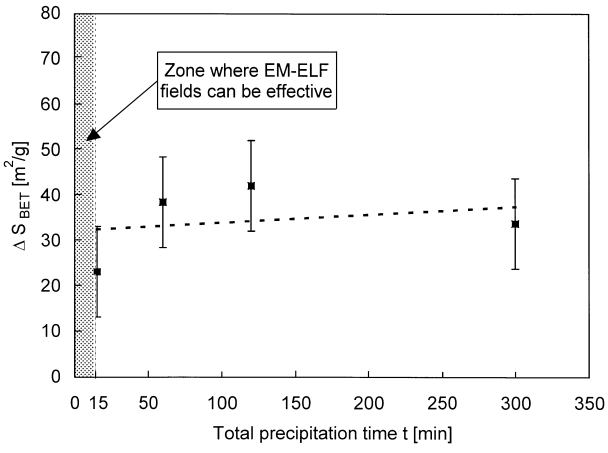

Fig. 10. Decrement in S_{BET} value, due to the effect of the EM-ELF field, versus total precipitation time.

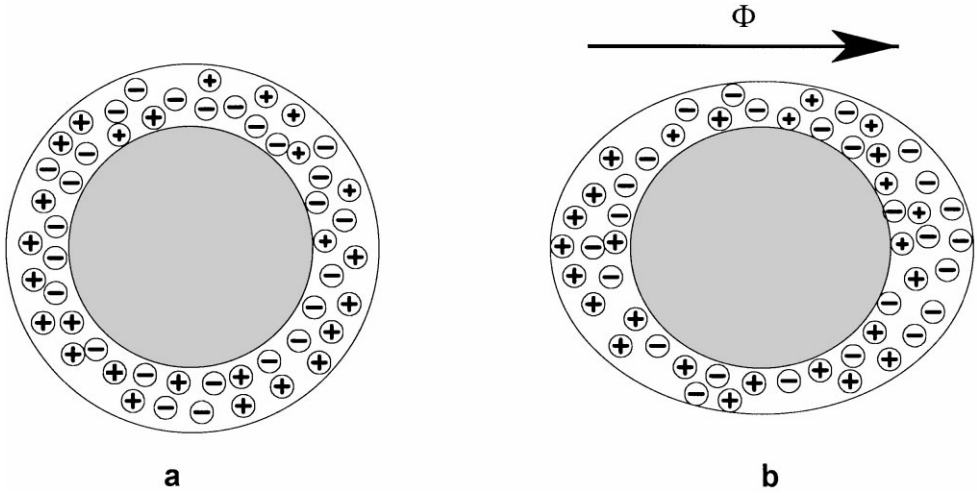

Fig. 11. Model to illustrate how EM-ELF field can strain the solid/liquid interface of a nucleus of critical size.

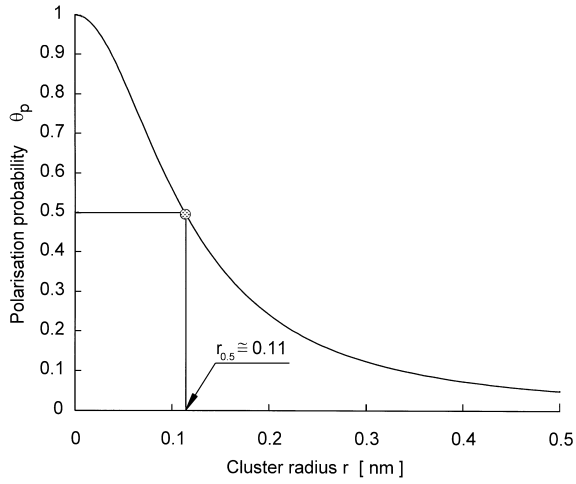

Fig. 12. Polarisation probability θ_p as a function of particles radius r.

For calcium phosphates compounds, the value of the water/solid interfacial energy can be set around 100 mJ m^{-2}.[35] As a matter of discussion let us plot (Fig. 12) the probability θ_p as a function of particles radius using the above reported data. As it is possible to observe, this probability reaches the value of 50% when the particles radius is 0·11 nm.

This dimension, accordingly to Prigogine,[33] might be associated with the dimension of the critical nuclei that are forming in a supersaturated solution prior the crystal growth steps. Without stressing too much the number derived in this discussion, it seems nevertheless reasonable that the EM-ELF applied fields are effective only at the very beginning of the nucleation process. The enhanced grains dimension observed experimentally should reflect the increasing in the interfacial solid/liquid energy of those initial nuclei of critical dimension for which, due to an increasing in their surface activity, their rate of crystal growth should be faster.[33] The effects of EM-ELF may be low, but nevertheless significant and possibly relevant.

4 Conclusions

1. In high supersaturating regime, the spontaneous precipitation processes from aqueous solutions of calcium chloride and sodium phosphates lead to a solid phase mixture formed by OCP and OHAp.
2. The precipitate powders obtained with and without the application of a EM-ELF field of intensity B equal to 3 mT and frequency ν equal to 1300 Hz have an equal chemical composition and are formed by porous agglomerates.
3. The porous agglomerates formed under the EM-ELF field have specific surface values and an average grains dimensions respectively lower (18–36%) and higher (40%) than the ones concerning the samples obtained when no EM-ELF fields have been applied.
4. The EM-ELF forces are interacting with colloidal-like particles during the first stage of the precipitation process.

Acknowledgements

F. Stomeo and S. Verrecchia provided useful contributions for the calculations of the electric field that has been assumed acting on the colloidal-like particles in solution when EM-ELF field are applied. Professors A. Chiabrera and B. Bianco gave their expertise in designing the experimental apparatus here used. Discussions with these researchers and with Professor L. Albanese on the results of this paper were very helpful. We are indebted to Mr C. Uliana for the SEM and TEM investigations. This work was partially supported by the Italian MURST (40%), by the University of Genoa and by the Consiglio Nazionale delle Ricerche contract no. 115.1538 and Progetto Finalizzato "Materiali Speciali per Tecnologie Avanzate II".

References

1. Beruto, D. T. and Giordani, M., Effects of low frequency electromagnetic fields on crystal growth from solutions. In *Research in Chemical Kinetics*, Vol. 3, ed. R. G. Compton and G. Hancock. Elsevier Science, Amsterdam, 1995, pp. 175–213.
2. Berton, R., Beruto, D. T., Bianco, B., Chiabrera, A. and Giordani, M., Effect of ELF electromagnetic exposure on precipitation of barium oxalate. *Bioelectrochem. and Bioenerg.*, 1993, **30**, 13–25.
3. Beruto, D. and Giordani, M., Calcite and aragonite formation from aqueous calcium hydrogencarbonate solutions: effect of induced electromagnetic field on the activity of $CaCO_3$ nuclei precursors. *J. Chem. Soc. Faraday Trans.*, 1993, **89**, 2457–2461.
4. Gilber, J., Göpel, W., Holmes, I. L., Horvai, G., Meixner, H. and Tímár-Horváth, (eds), *Proceedings of EUROSENSORS VII*, Elsevier Science, Lausanne, 1994.
5. Park, J. B. and Lakes, R. S., *Biomaterials: An Introduction*, 2nd ed. Plenum Press, New York, 1992.
6. Feenstra, T. P. and De Bruin, P. L., Formation of calcium phosphates in moderately supersaturated solutions. *J Phys. Chem.*, 1979, **83**, 475–479.
7. Nancollas, G. H. and Tomazic, B., Growth of calcium phosphate on hydroxyapatite crystals. Effect of supersaturation and ionic medium. *J. Phys. Chem.*, 1974, **78**, 2218–2225.
8. Francis, M. D. and Webb, N. C., Hydroxyapatite formation from a hydrated calcium monohydrogen phospate precursor. *Calc. Tiss. Res.*, 1971, **6**, 335–342.
9. Beruto, D., Reactions at nanometric solid–liquid interfaces influenced by low frequency electromagnetic fields and microstructure development of the precipitates. In

Ceramic Microstructure. Control at Atomic Level, ed. A. P. Tomsia and A. M. Glaser. Plenum Press, New York, 1998, pp. 429-436.
10. Best, S., Characterisation, sintering and mechanical behaviour of hydroxyapatite ceramics. Ph.D. thesis, University of London, 1990.
11. Basset, C. A. L., Fundamental and practical aspects of therapeutic uses of pulsed electromagnetic fields (PEMFs). *Critical Reviews in Biomedical Engineering*, 1989, **17**(5), 451–529.
12. Basset, C. A. L., Therapeutic uses of electric and magnetic fields in orthopaedics. In *Biological Effects of Electric and Magnetic Fields*, Vol 2, ed. D. O. Carpenter and S. Ayrapetyan. Academic Press, San Diego, CA, 1994, pp. 13–47.
13. Black, J., *Electrical Stimulation. Its Role in Growth, Repair, and Remodeling of the Muscoloskeletal System*. Praeger, New York, 1987.
14. Chiabrera, A., Nicolini, C. and Schwan. H. P. (eds), Interactions between Electromagnetic Fields and Cells. NATO ASI Serie A, Vol 97. Plenum Press, New York, 1985.
15. Bianco, B. and Chiabrera, A., From the Langevin–Lorentz to the Zeeman model of electromagnetic effect on ligand–receptor binding. *Bioelectrochem. and Bioenerg.*, 1992, **28**, 355–361.
16. Elliot, J. C., *Structure and Chemistry of Calcium Apatite and other Calcium Orthophosphates*. Elsevier, Amsterdam, 1994.
17. Anderson, H. C., Biology of disease. *Mechanism of mineral formation in bone. Laboratory Investigation*, 1989, **60**, 320–330.
18. Uchida, A., Nade, S. M. L., McCartney, E. R. and Ching, W., The use of ceramics for bone replacement. *J. of Bone and Joint Surgery*, 1984, **66B**, 269–275.
19. lijima, M., Kamemizu, H., Wakamatsu, N., Goto, T., Doi, Y. and Moriwaki, Y., Precipitation of octacalcium phosphate at 37°C and at pH 7.4 in relation to enamel formation. *J. Cryst. Growth*, 1991, **112**, 467–73.
20. Beruto, D., Botter, R. and Searcy, A. W., H_2O-catalized sintering of ≈2-nm-cross-section particles of MgO. *J. Amer. Ceram. Soc.*, 1987, **70**, 155–159.
21. Sanders, V., Catalysis. In *Science and Technology*, ed. J. R. Anderson and M. Boudart. Springer–Verlag, Berlin and Heidelberg, Vol. 7, 1985, pp. 51–158.
22. Lowell, S., *Introduction to Powder Surface Area*. Wiley-Interscience, New York, 1979.
23. Gregg, S. J. and Sing, K. S. W., *Adsorption, Surface Area and Porosity*. Academic Press, London, 1982.
24. De Boer J. H., Linsen B. G. and Osinga, T. J., Pore Systems in Catalists: VI.. *J Catal.*, 1965, **4**, 643–648.
25. Blazek, A., *Thermal Analysis*. Van Nostrand Reinhold, London, 1973.
26. *JCPDS*. International Centre for Diffraction Data, ed. W. F. McClune. Newtown Square, Pennsylvania, PA, 1996.
27. Constantz, B. R., Ison, I. C., Fulmer, M. T., Poser, R. D, Smith, S. T., Van Wagoner, M., Ross, J., Goldstein, S. A., Jupiter, J. B., Rosenthal, D. I. Skeletal repair by in situ formation of the mineral phase of bone Science., 1995, **267**, 1796–1798.
28. Beruto, D., Barco, L., Belleri, G. and Searcy, A. W., Vapor-phase hydration of submicrometer CaO particles. *J. Amer. Ceram. Soc.*, 1981, **64**, 74–80.
29. Vogel, A. I., *A Text Book of Quantitative Inorganic Analysis*. Longman, London, 1961.
30. Beruto, D., Barco, L. and Searcy, A. W., CO_2-catalyzed surface area and porosity changes in high-surface-area CaO aggregates. *J. Amer. Ceram. Soc.*, 1984, **67**, 512–515.
31. Orr, C. and Dalla Valle, J. M., Fine Particle Measurement. Maemillan, New York, 1959.
32. Underwood, E. E., *Quantitative Stereology*. Addison–Wesley, London, 1970.
33. Defay, R., Prigogine, I., Bellemans A. and Everett, D. H., *Surface Tension and Adsorption*, Longman, London, 1966.
34. Stomeo, F. and Verrecchia, S., Interazioni tra esposizione EM-ELF e precipitazione di fosfati di calcio di interesse biologico. Thesis, University of Genoa, Italy, 1996.
35. Nielsen A. E., *Crystal Growth*. Pergamon, Oxford, 1967.